

Chemical enrichment by collapsars as the origin of the unusually high [Ba/Fe] in a massive star cluster of the dwarf galaxy NGC 1569

Brayden Leicester,^{1,2*} Kenji Bekki¹ Takuji Tsujimoto³

¹ICRAR M468 The University of Western Australia 35 Stirling Hwy, Crawley Western Australia 6009, Australia

²School of Physical and Chemical Sciences, University of Canterbury, Private Bag 4800, Christchurch 8140, New Zealand

³National Astronomical Observatory of Japan, Mitaka-shi, Tokyo 181-8588, Japan

Accepted XXX. Received YYY; in original form ZZZ

ABSTRACT

The super star cluster NGC1569-B has recently been observed to have an extremely high [Ba/Fe]. We consider that the observed high [Ba/Fe] (~ 1.3) is due to the chemical enrichment of giant molecular clouds by either collapsars, neutron star mergers, or magneto-rotational supernovae, and thereby investigate which of the three polluters can best reproduce the observed [Ba/Fe]. Since it is found that collapsars can best reproduce such an extremely high Ba abundance, we numerically investigate the star cluster formation in NGC1569 using chemodynamical simulations of merging dwarf galaxies with chemical enrichment by collapsars. The principal results are as follows. First, a cluster of the same scale as NGC1569-B was found to match both the observed [Ba/Fe] and [Fe/H] values, the best cluster having [Ba/Fe] = 1.3 ± 0.2 and [Fe/H] = -0.7 ± 0.2 . This simulation used a core-collapse supernova per collapsar rate of 70, a standard initial mass function and an initial metallicity of [Fe/H] = -1.5 . Second, a prediction of the Eu abundance of NGC1569-B is made: [Eu/Fe] = 1.9 ± 0.2 . These results are shown to be invariant under a change in the orbit parameters used for the merger. The need for a merger to promote the star formation that leads to the synthesis of the Ba and the star cluster formation is confirmed. Collapsars can not only better explain [Ba/Fe] but also be consistent with the observed star formation rate and stellar mass of the dwarf galaxy.

Key words: galaxies: star clusters: individual: NGC1569-B – software: simulations

1 INTRODUCTION

Recent photometric and spectroscopic observations of the Galactic globular clusters (GCs) have revealed that the GCs have internal abundance spreads in light (Osborn 1971; Sneden et al. 1992; Gratton et al. 2004; Meléndez & Cohen 2009), s-process (e.g. Marino et al. 2009), and r-process elements (e.g. Roederer 2011). These observations also have discovered intriguing anti-correlations between O and Na (Sneden et al. 1992; Carretta et al. 2009, 2010; Gratton et al. 2015), C and N (e.g. Bell & Dickens 1980), Mg and Al (Pancino et al. 2017, e.g.), and K and Mg (Mucciarelli et al. 2012; Carretta & Bragaglia 2021), which can possibly provide strong constraints on the theories of GC formation. These all imply there are multiple chemical populations in most GCs, which are not present in young massive clusters (YMCs) (Gratton et al. 2012; Bastian & Lardo 2018). MPs are important to understand as they are key links to the formation history of the GC due to the different processes that produce each trend.

Of concern to this work are the rapid neutron capture (*r*-)process elements (Arnould et al. 2007; Cowan et al. 2021). The spread in these *r*-process elements were reviewed across many galactic GCs by Roederer (2011). Since then, the cluster M15 has been repeatedly observed. A bimodal spread in Ba (and other *r*-process elements) was found (Worley et al. 2013), and there was no trend in this dispersion

with stellar luminosity (Kirby et al. 2020), so the Ba must have been made before or during the cluster formation. This constrains the timescale of the events used to do the pollution. M92 had *r*-process dispersion in only the first generation of stars, with the younger generation showing no variation (Kirby et al. 2023), which indicates that the pollution occurs within a short time of the birth of the first generation, and with a delay in the second generation to allow for the mixing of the *r*-process elements.

Recently a super star cluster (SSC) NGC1569-B has been observed to have an over-abundance of Ba, [Ba/Fe] = 1.28 ± 0.21 (Gvozdenko et al. 2022, hereafter G22) using an integrated light spectrum. They also report a [Fe/H] = -0.74 ± 0.05 . This Ba abundance is much higher than anything measured previously and requires further study to try and recreate a star cluster with [Ba/Fe] so super solar. The [Ba/Fe] reported in G22 is seemingly independent of their changing the ratio of red to blue supergiants. With such an invariant value under such a change and the extremely super solar nature of the Ba abundance, this work uses the largest uncertainty given, ± 0.21 . The attempted explanation in G22 for this high [Ba/Fe] from asymptotic giant branch (AGB) stars synthesising Ba through the slow neutron capture (*s*-)process is unsatisfying, as the authors admit because the AGB pollution timescale is larger than the cluster age.

NGC1569 is a blue compact dwarf (BCD) galaxy (Israel 1988). There are two SSCs inside NGC1569, labelled -A and -B. This work focuses on NGC1569-B, which has an age of 15 – 25 Myr (Larsen et al. 2007). The star formation history (SFH) of NGC1569 has been

* E-mail: brayden.leicester@canterbury.ac.nz (BL)

a complicated one, [Angeretti et al. \(2005\)](#) concluded that it is most likely that there have been three periods of intense star formation (SF) in the last 1 – 2 Gyr, the youngest of which occurred between 37 and 13 Myr ago. This is corroborated by [McQuinn et al. \(2010\)](#), which has a burst occurring for most of the last ~ 100 Myr, and [Anders et al. \(2004\)](#) found a burst starting around 25 Myr ago, in agreement with the SSC age. The outer region of this galaxy has been consistently forming stars for the whole Hubble time, as shown by [Grocholski et al. \(2012\)](#). This relatively constant SF is thought to have ceased ~ 0.5 Gyr ago, and the bursts come after this. The stellar population with an age > 10 Gyr has a considerable [Fe/H] spread from -1 to -2. This older population has a uniform spatial distribution, unlike concentrated newer stars ([Aloisi et al. 2001](#)). The distance to NGC1569 used in these works was often quoted as (2.2 ± 0.6) Mpc, citing [Israel \(1988\)](#). [Grocholski et al. \(2012\)](#) disagree, based on their earlier work ([Grocholski et al. 2008](#)), with new data that resolves the tip of the red giant branch, finding a distance of (3.06 ± 0.18) Mpc. [Grocholski et al. \(2008\)](#) showed that any measurements of the SF rate (SFR) were too small because of the shorter distance used. The distance change updates the mass of NGC1569-B from [Larsen et al. \(2007\)](#) to $6.1 \times 10^5 M_{\odot}$. [Hunter & Elmegreen \(2004\)](#) uses another distance of 2.5 Mpc, citing [O’Connell et al. \(1994\)](#). The distance corrected value for SFR becomes $0.48 M_{\odot} \text{ yr}^{-1}$. This value is used for all further SFR calculations. The SFR surface density, Σ_{SFR} , invariant with distance, is tabulated at $1.29 M_{\odot} \text{ yr}^{-1} \text{ kpc}^{-2}$ ([Hunter & Elmegreen 2004](#)). A merger or interaction in the NGC1569-B’s past is likely, such as the ones described in [Johnson \(2013\)](#) or [Stil & Israel \(1998\)](#). This merger scenario explains the starburst ([Schweizer 2005](#); [Barnes 2004](#)). The SFH is consistent with the general case of a bursty SF period during a merger ([Cortijo-Ferrero et al. 2017](#)) and the drop in SFR after the merger ([Pearson et al. 2019](#)).

There have been attempts made to simulate the observed dispersion of *r*-process elements in galactic GCs. [Bekki & Tsujimoto \(2017\)](#) uses a model where the higher *r*-process abundances are in a second generation of stars, whereas [Tarumi et al. \(2021\)](#) use a single *r*-process polluting event before the cluster forms. Both of these use neutron star mergers (NSMs) as the polluter. Also, they use Eu as the tracer of the *r*-process, not Ba, because of the possible *s*-process origin of the Ba. Eu was not measured in [G22](#). [Tsujimoto et al. \(2017\)](#) measure both Ba and Eu, along with Y, and explain the enrichment of dwarf spheroidal galaxies with both NSMs and magneto-rotational supernovae (MR-SNe). These models explain very subsolar abundances, unlike the observations of [G22](#) being investigated here. All the *r*-process elements in these models are often hypothesised to be made in a single event, due to the low abundances being explained. Because the [Ba/Fe] of NGC1569-B is so supersolar, all forms of *r*-process Ba pollution need to be considered, as well as multiple events. The standard NSMs and MR-SNe are considered, as well as a different polluter, collapsars (COLs) ([MacFadyen & Woosley 1999](#)). These are another type of supernova of rotating massive stars that have higher *r*-process yields ([Siegel et al. 2019](#)). [G22](#) was the first [Ba/Fe] measurement made of NGC1569-B, and this work is the first attempt to model the extremely high value measured. The different *r*-process yields and time scales of the three pollution sites ([Siegel 2022](#)) can be used to distinguish which of them is the dominant polluter of this cluster, as the [Ba/Fe] is so high.

The purpose of this paper is to reproduce a cluster with similarly high [Ba/Fe] based on new computer simulations of GC formation, incorporating chemical enrichments of the interstellar medium (ISM) by collapsars in merging between gas-rich dwarf galaxies. We particularly investigate the mean [Ba/Fe] of stars in the simulated star clusters (SCs) and the internal [Ba/Fe] spread among the SC member

stars for each SC. Although we have already investigated SC formation in interacting (e.g. [Bekki et al. 2004](#); [Williams et al. 2022](#)) and merging galaxies (e.g. [Bekki et al. 2002](#)), we did not investigate the Ba abundance properties of the simulated SCs. Therefore, our new simulations can provide new clues to the origin of SCs with unusually high [Ba/Fe] formed in dwarf-dwarf merging. Our previous simulations also showed that secondary star formation from gas accreted onto existing SCs is possible (e.g. [Bekki & Mackey 2008](#); [McKenzie & Bekki 2018](#)), which means that [Ba/Fe] of second-generation stars can be quite high if new stars are formed from accreting gas mixed with Ba-rich ejecta from low-mass AGB stars. However, we do not consider this possibility in this paper at all, because the SCs in NGC1569 are so young that such AGB stars are unlikely to contribute to early chemical enrichment in SC formation. Although there are several recent simulations on the SC formation and chemical abundance patterns of the simulated SCs (e.g. [Lahén et al. 2024](#)), we do not discuss these results much, because we focus exclusively on the [Ba/Fe] of SCs in BCD galaxies.

This paper is laid out as follows: The model is presented in [section 2](#), with the three *r*-process polluters discussed in turn in [subsection 2.1](#), the simulations of the best polluter are then described for the rest of the section. In [section 3](#) we present the fiducial model from our simulations and discuss the properties of this chosen cluster and how the results are affected by a change in the parameters of the merger. These results are further discussed and put in context in [section 4](#). The key takeaways and a conclusion are presented in [section 5](#).

2 THE MODEL

We consider that collapsars, neutron star mergers, and magneto-rotational supernovae could all possibly pollute the ISM of the dwarf galaxy with their ejecta rich in *r*-process elements in the present study. Core-collapse supernovae (CCSNe) have long been speculated to be *r*-process sites, along with NSMs, but there is great debate over the contribution for each kind of site (summarised in [Siegel 2022](#)).

We first investigate the required numbers of COLs, NSMs and MR-SNe (N_{COL} , N_{NSM} , $N_{\text{MR-SN}}$ respectively) that are needed to pollute the ISM to the observed level. Then, from these N_{COL} etc., we derive the required masses of all stars including these polluters ($M_{*,\text{COL}}$, $M_{*,\text{NSM}}$, $M_{*,\text{MR-SN}}$) for a given set of parameters for stellar initial mass functions (IMFs) and fractions of such particle types of explosive events among stellar populations. By doing so, we can investigate (i) whether $M_{*,\text{COL}}$ etc. are possible for such a small dwarf galaxy like NGC1569 thus (ii) which of the three is the most reasonable polluter for of Ba for this cluster.

Then we perform computer simulations with chemical enrichment by the best polluter and attempt to find a SSC similar NGC1569-B in [Ba/Fe], [Fe/H] and mass. These simulations vary physical parameters of the system, that can be linked back to observables. We consider that this two-stage investigation is the best way to understand the origin of rather high [Ba/Fe] that was found by [G22](#), because it is extremely time-consuming to investigate all of these three possibilities using numerically costly computer simulations of dwarf galaxy mergers.

2.1 Three Possible Polluters

2.1.1 Collapsars

COLs are a well-studied subset of CCSNe, first postulated as “failed” supernova ([Woosley 1993](#)) because the explosion happens slightly

delayed from the core-collapse, often as a (long) gamma-ray burst (GRB) (Woosley & Bloom 2006). The Ba that COLs produce is made through the r -process. An accretion disk is formed around the black hole that occurs when the core-collapse marks the death of the COL progenitor. This disk becomes opaque to the neutrinos it produces, which starts a feedback loop that is a long theorised (Pruet et al. 2004; McLaughlin & Surman 2005; Kohri et al. 2005; Siegel et al. 2019; Miller et al. 2020; Zenati et al. 2020; Brauer et al. 2021; Barnes & Duffell 2023) site of nucleosynthesis through the r -process. However, recent observations of some supernovae (Anand et al. 2024) and a GRB (Blanchard et al. 2024) are not finding signatures of the r -process, although these signatures should exist (Barnes & Metzger 2022). This does throw some doubt on the COL model of r -process pollution, but more work is needed in this area. The accretion disk in a COL also powers the jets and the resulting explosion of a GRB (MacFadyen et al. 2001) or jet driven supernova (Heger et al. 2003). COLs form more heavy r -process elements than NSMs by up to 30 times the yield (Siegel et al. 2019), and can be thought of as the dominant polluter of the ISM for these species, especially on short time scales. A lower metallicity increases the chance of COLs because Wolf-Rayet (WR) stars wind-driven mass loss increases with metallicity (Crowther 2007) and some stripping is necessary for a GRB, but an excess leads to lower angular momentum and therefore fewer COLs (Fryer et al. 1999). The envelope stripping could also be done by a binary companion, with $\sim 70\%$ of O stars in binaries (Sana et al. 2012) the chances of a COL occurring increases. Because their progenitors are massive stars, COLs can reasonably be assumed to happen without a large delay, as their main sequence (MS) lifetime is only a few Myr.

To calculate the number of COLs, N_{COL} , needed to pollute a GMC to the extreme level of [Ba/Fe] being investigated, the initial metallicity of the system is used to get the initial Ba concentration, and thus an initial mass of Ba, $M_{\text{Ba},i}$. This is then incremented by the yield of Ba from a single COL, $m_{\text{ej},\text{Ba},\text{COL}}$, until the [Ba/Fe] matches that of the observation G22. The yields used here are those needed to reproduce galactic abundances, from Siegel et al. (2019). The Ba produced in each COL will not all go into the GMC, as this depends on where the COL occurs, the recycling efficiency of the ISM, and many other unknowns. The fraction of Ba retained by the GMC is denoted f_{ret} , the retention parameter. $f_{\text{ret}} = 1$ implies all the Ba from every COL goes into the SSC. This is unphysical as while the ejecta may not escape the galaxy, not all the ejecta from each event will go into the one GMC that eventually forms the SSC, so smaller values of f_{ret} are used. This leads to the final mass of Ba, $M_{\text{Ba},f}$, which can be found by

$$M_{\text{Ba},f} = M_{\text{Ba},i} + m_{\text{ej},\text{Ba},\text{COL}} \cdot f_{\text{ret}} \cdot N_{\text{COL}}. \quad (1)$$

Allowing for all the ways r -process COL ejecta could not make it to a GMC with an $f_{\text{ret}} = 0.1$, equation (1) can be inverted for the number of COLs. The solid purple line in Fig. 1 shows this, with the cumulative addition of Ba from COLs far outpacing NSMs and MR-SNe. This has been done under some fairly generous assumptions: COLs don't add Fe to the system, nor do any other CCSN, and the metallicity of the system stays constant at the observed [Fe/H] = -0.74 G22. The rates of the other polluters will get the same generosity.

$$N_{\text{CCSN}} = N_{\text{COL}} \cdot f_{\text{COL}}. \quad (2)$$

Multiplying the number of COLs by an appropriate ratio of CCSN per COL, f_{COL} , (a key parameter of the simulations, see subsection 2.4.1 below for a larger discussion of this parameter) gives the number of CCSN needed, N_{CCSN} , as shown in equation (2). A

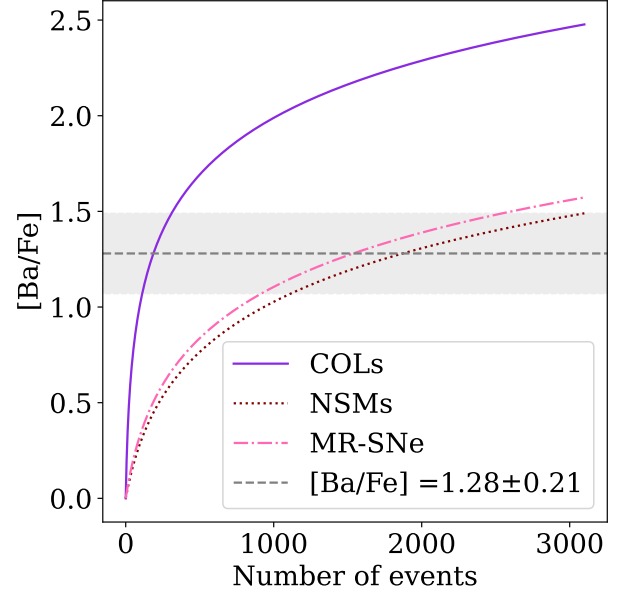


Figure 1. The cumulative [Ba/Fe] for the three different types of polluters increasing with the number of events. COLs (solid purple line) are far more efficient at increasing the Ba abundance than either the NSMs (dotted brown line) or MR-SNe (dot-dashed pink line), due to the higher $m_{\text{ej},\text{Ba}}$. The observed value of [Ba/Fe] in NGC1569-B (1.28 ± 0.21 , G22) is shown by the dashed grey line for the value and the rectangle for the uncertainty.

conservative value of $f_{\text{COL}} = 1000$ is used for this calculation. Integrating over all the high-mass stars that can undergo a CCSN ($8 M_{\odot}$ to $50 M_{\odot}$), the fraction of CCSN per unit solar mass is found by

$$N_{\text{CCSN},0} = C_{\text{IMF}} \int_{8 M_{\odot}}^{50 M_{\odot}} \phi(m) dm. \quad (3)$$

equation (3) uses a normalised (Salpeter 1955) initial mass function (IMF), $\phi(m) = C_{\text{IMF}} m^{-\alpha}$ with slope α , with C_{IMF} being the normalisation constant which comes from integrating over all possible stellar masses

$$1 = C_{\text{IMF}} \int_{0.1 M_{\odot}}^{50 M_{\odot}} \phi(m) m dm. \quad (4)$$

The mass of stars that need to form are given by

$$M_{*,\text{COL}} = \frac{N_{\text{CCSN}}}{N_{\text{CCSN},0}}. \quad (5)$$

Using an SFR (the $0.48 M_{\odot} \text{ yr}^{-1}$ from Hunter & Elmegreen 2004) the time to form this mass of stars, $\Delta t_{\text{SF},\text{COL}}$, is found by

$$\Delta t_{\text{SF},\text{COL}} = \frac{M_{*,\text{COL}}}{\text{SFR}}. \quad (6)$$

The values are calculated to be $M_{*,\text{COL}} = 2.6_{-1.1}^{+1.7} \times 10^7 M_{\odot}$ of stars need to form, which takes $\Delta t_{\text{SF},\text{COL}} = 53_{-22}^{+36}$ Myr by equation (5) and equation (6). The slight dispersion in the lifetimes of these COLs and the SF being an extended event on these timescales means the COLs could all pollute the same GMC, which can live for ≈ 10 Myr (Mouschovias et al. 2006). This time of star formation fits well with the SFH of NGC1569 Angeretti et al. (2005), which used higher but less certain SFRs which would only decrease the time of star formation. So the collapsar model makes sense for this pollution of

Ba. These values depend on the slope of the IMF chosen, and we investigate changing the IMF to an SFR-dependent one during the simulations.

2.1.2 Neutron Star Mergers

NSMs were observationally confirmed by their gravitational wave signature (Abbott et al. 2017) and have been used to explain the r -process pollution for a long time, see the models in other works discussed above for more information. They have often been invoked as single-event polluters, but the extreme [Ba/Fe] being investigated here requires many NSM events. We now calculate how many NSMs are expected in NGC1569 from the old stellar population, and the number needed to raise the [Ba/Fe] to the necessary level.

Because of the long time delay, the mass of stars that need to form for the NSM pollution, $M_{*,\text{NSM}}$, cannot be calculated. However, the number of NSMs that occur at a given time from the old stellar population of NGC1569 in some change in time Δt can be calculated. The NSMs from this population are proportional to a few quantities related to the number of NS binaries. The binary star fraction, here assumed to be 50%, this comes from the Sana et al. (2012) binary fraction of 70% and their claim that at least 20% of these will result in mergers for the O-type stars while they are still on the main sequence. These values are also adopted for the early B type stars that can become neutron stars. The fraction of stars that form neutron stars $N_{\text{NS},0}$, here taken to be the number of stars made between $8 M_{\odot}$ to $20 M_{\odot}$, is also important.

$$N_{\text{NS},0} = C_{\text{IMF}} \int_{8 M_{\odot}}^{20 M_{\odot}} \phi(m) dm \quad (7)$$

This uses the same C_{IMF} as found in equation (4), and calculates the fraction of stars in that mass range, so equation (7) is much like equation (3). Also normalising an NS merger function

$$1 = C_{\text{NSM}} \int_{0 \text{ Gyr}}^{13 \text{ Gyr}} \frac{t_{\text{min}}}{t} dt \quad (8)$$

to solve for C_{NSM} as the normalisation constant, with $t_{\text{min}} = 700 \text{ Myr}$ as the minimum delay time of an NSM. Having all the mergers occur during the lifetime of the galaxy so far is generous because there is no reason they should have all occurred already. Integrating this same function as in equation (8) over the $\Delta t = 10 \text{ Myr}$ lifetime of a GMC (Mouschovias et al. 2006) at the galaxies' current age (13 Gyr, Grocholski et al. 2012)

$$N_{\text{NSM},0} = 0.5 \cdot C_{\text{NSM}} \cdot N_{\text{NS},0} \int_{13 \text{ Gyr}}^{13.01 \text{ Gyr}} \frac{t_{\text{min}}}{t} dt \quad (9)$$

gives a number of NSM per solar mass in this Δt , where the 0.5 coefficient comes from the 50% binary fraction. Multiplying this value by the mass of stars in the galaxy, $M_* = 2.8 \times 10^8 M_{\odot}$ (Johnson et al. 2012) gives 84 NS mergers occurring in NGC1569 when the SSC was forming. This is galaxy-wide, so not all the r -process Ba synthesised by these events will be incorporated into the GMC.

The number of NS mergers needed to reach the high [Ba/Fe] measured by G22 can be calculated similarly to the number of COLs needed. By replacing the N_{COL} values with N_{NSM} parameters in equation (1), the N_{NSM} value can be calculated. Once again an f_{ret} is applied to account for all the ways that the Ba does not make it to the GMC. For consistency, $f_{\text{ret}} = 0.1$ has been used for NSMs as well. The [Ba/Fe] increase with N_{NSM} is shown in Fig. 1 for NSMs (in dotted brown) too. It is no accident that an order of magnitude more

NSMs are needed over the COLs. The yields used have been $\times 10$ less than the COL yield, as suggested by Siegel et al. (2019), (i.e. $m_{\text{ej,Ba,NSM}} = 0.1 \cdot m_{\text{ej,Ba,COL}}$). The N_{NSM} estimated from Fig. 1 is clearly more than the 84 NSMs that occur in $\Delta t = 10 \text{ Myr}$ from the 13 Gyr age of this population. This same mass of ‘‘old’’ stars would need to be only 600 Myr old for NSMs to be viable polluters (setting this as the lower bound of integration in equation (9) with the same Δt), for this yield and f_{ret} combination. The mass of stars formed in the bursty star formation in the last Gyr is too small, by an order of magnitude, to apply the same argument of NSM pollution from the younger stars.

2.1.3 Magneto-Rotational Supernovae

A similar analysis to the COLs and NSMs can be done for magneto-rotational supernovae. This calculation is shown in Fig. 1 with the dot-dashed pink line for MR-SNe. The Ba ejected per event, $m_{\text{ej,Ba,MR-SN}}$, was calculated by Nishimura et al. (2017) (but see also Tsujimoto et al. 2017) and used for the substitution into the MR-SNe equivalent of equation (1). Once again, $f_{\text{ret}} = 0.1$ is used, so the results are comparable with the other polluters.

The MR-SNe are closer to the NSMs than the COLs for the number needed, as inferred from Fig. 1. N_{CCSN} can be calculated from a parallel to equation (2), the value of $N_{\text{MR-SN}}$ and a CCSN per MR-SN value of $f_{\text{MR-SN}} = 200$ (Tsujimoto et al. 2015). With this value and the same $N_{\text{CCSN},0}$ from equation (3), $M_{*,\text{MR-SN}}$ can be calculated in an analogous way to equation (5). This implies $M_{*,\text{MR-SN}} = 4.3^{+2.8}_{-1.8} \times 10^7 M_{\odot}$, which would be an SF time of $\Delta t_{\text{SF,MR-SN}} = 90^{+58}_{-38} \text{ Myr}$ from an adjustment of equation (6). Even with MR-SN being a higher fraction of all CCSN than the COL fraction estimate, it is unlikely that these events will be numerous enough for the pollution of Ba in NGC1569-B, as the SF time and mass of stars needed is not in agreement with the observations. There is also debate over the r -process production rates in MR-SNe, with Mösta et al. (2018) arguing that the magnetic fields need to be larger than is realistic, else the r -process production is reduced by two orders of magnitude above the 2nd peak.

2.1.4 The Best Polluter

From the above analysis, nicely captured in Fig. 1, COLs are the only polluter that could have raised the progenitor GMC of NGC1569-B to a [Ba/Fe] as high as it has been observed (G22). The mass of new stars and the time taken to form them are broadly consistent with the SFH in the COL scenario. MR-SNe are close to being able to reproduce the measurements, but the SF time is too long. There are not enough NSMs occurring due to the old stellar population to provide the needed NSMs for pollution of [Ba/Fe] up to ~ 1.3 . Thus, collapsars are used as the polluter for the simulations of the SSC formation described below.

2.2 Initial disk models

Since our previous simulations demonstrated that BCDs like the host dwarf galaxy NGC 1569 can be formed from mergers between bulgeless and gas-rich dwarf disk galaxies (Bekki 2008), we here adopt the gas-rich disk galaxy models for merger progenitor galaxies. We here briefly describe the disk models, given that the details of the disk models have been described in our previous papers (Bekki 2008, 2014). A dwarf galaxy is assumed to consist of dark matter, stars, and gas (without stellar bulge). The total masses of dark matter

halo, stellar disk, and gas disk in a dwarf galaxy are denoted as M_{dm} , M_{s} , M_{g} , respectively. In order to describe the radial density profile of the dark matter halo of the dwarf galaxy, we adopt the density distribution of the NFW halo (Navarro et al. 1996) suggested from CDM simulations:

$$\rho(r) = \frac{\rho_0}{(r/r_s)(1+r/r_s)^2}, \quad (10)$$

where r , ρ_0 , and r_s are the spherical radius, the characteristic density of a dark halo, and the scale length of the halo, respectively, and the reasonable value of the central concentration parameter, c ($c = r_{\text{vir}}/r_s$, where r_{vir} is the virial, predicted from NFW) is given to each low-mass dark matter halo in the present study (i.e., larger c for larger M_{dm}). We mainly investigate the models with $M_{\text{dm}} = 10^{11} M_{\odot}$, $R_{\text{vir}} = 45 \text{ kpc}$, $c = 16$, $M_{\text{s}} = 6 \times 10^8 M_{\odot}$, and $M_{\text{g}} = 1.2 \times 10^9 M_{\odot}$, which is a reasonable set of parameters for the dwarf galaxy NGC 1569.

The radial (R) and vertical (Z) density profiles of an initially thin stellar disk with a disk size R_s are proportional to $\exp(-R/R_0)$ with scale length $R_0 = 0.2R_s$ and to $\text{sech}^2(Z/Z_0)$ with scale length $Z_0 = 0.04R_s$, respectively, in all dwarf galaxy models. The gas disk with a size $R_g = 2R_s$ is also assumed to have a scale length of $R_{0,g}$ and a vertical scale length $Z_{0,g}$. In addition to the rotational velocity caused by the gravitational field of stellar and gaseous disk, bulge, and dark halo components, the initial radial and azimuthal velocity dispersions are assigned to the disc component according to the epicyclic theory with Toomre's parameter $Q = 1.5$ for all dwarf galaxy models. The vertical velocity dispersion at a given radius is set to be 0.5 times as large as the radial velocity dispersion at that point. We investigate only the thin disk models with $R_s = 5 \text{ kpc}$ (i.e., $R_0 = 1 \text{ kpc}$) in the present study, though the results might depend on the initial disk structures and kinematics. A stellar bar, which can possibly trigger a central starburst, cannot be formed from gravitational instability in the initial disks, because the initial stellar disk fractions are very small (≈ 0.006 , i.e., very weakly self-gravitating).

In order to investigate chemical enrichment, star formation, and dust formation and evolution in dwarf-dwarf mergers, we adopt the same code and model as those used in our previous studies that investigated metal and dust enrichments in galaxies (Bekki 2013, hereafter B13, Bekki (2015)). Since the details are given in B13, we here briefly describe the models. The only minor difference between this study and B13 is that the time evolution of Ba and Eu in galaxies is newly investigated in the present chemodynamical simulations: it should be stressed here that dust-phase Ba and Eu abundances are not considered in the present study due to the lack of knowledge about their depletion levels in ISM. Galaxy-wide star formation in dwarf mergers is based on the observed Kennicutt-Schmidt law, i.e., $\text{SFR} \propto \rho_{\text{g}}^{\alpha_{\text{sf}}}$ (Kennicutt 1998), where α_{sf} is the slope of the power-law and set to be 1.5 in the present study, as observed. Conversion from gas particles into new collisionless stellar particles is assumed to occur if the local density exceeds a threshold density for star formation (ρ_{th}). As described later, this threshold gas density can have an influence on the final [Ba/Fe] of the simulated SCs. Feedback effects from CCSNe and SNIa are both incorporated, though those from NSMs are yet to be done. The same chemical yields from CCSNe, SNIa, and AGB stars as those used in B13 are adopted in the present study for the Salpeter IMF (Salpeter 1955). The model parameters for dust formation, growth, and destruction (e.g., dust yields and growth timescale) adopted in the present study are exactly the same as those in B13. Initial [Fe/H] are assumed to be free parameters so that the best initial [Fe/H] can be derived to explain the observed final [Ba/Fe] and [Fe/H] of NGC1569-B.

2.3 Orbital parameters for mergers

The orbit of a dwarf-dwarf merger is assumed to be parabolic with an orbital eccentricity of 1.0 in all models. The apocenter and pericenter (R_p) distances are set to be $10R_s$ (i.e., ten times the stellar disk size) and $0.1R_s$, respectively, in most models. The mass-ratio of two dwarfs represented by m_2 is a free parameter that can influence the strength of a starburst and the associated SC formation. We mainly investigate the major merger models with $m_2 = 1$. The orbit of the two dwarfs is set to be the xy plane and the spin of each galaxy in a merger is specified by two angles θ_i and ϕ_i , where suffix i ($=1$ and 2 , i.e., primary and companion galaxies) is used to identify each galaxy. θ_i (in units of degrees) is the angle between the z -axis in the adopted coordinate system and the vector of the angular momentum of a disc. ϕ_i is the azimuthal angle measured from the x -axis to the projection of the angular momentum vector of a disc onto the xy plane (i.e., orbital plane). We mainly show the results of a major merger model with $\theta_1 = 30$, $\theta_2 = 45$, $\phi_1 = 30$, and $\phi_2 = 120$ in the present study, though the orbital configurations can slightly influence SC formation processes.

2.4 Parameters for Collapsars

It is clear from the above analytical tests that the COLs are the only viable way of polluting Ba to the needed levels. So the simulations below use COLs as the polluter of r -process elements. Here we describe some parameters of the simulations that get changed in our suite of models.

2.4.1 CCSN per COL

There is a lot of debate around the rates of COLs. Converting the values given in other works to the simulation input value of CCSN per COL, how many massive stars there are before one of them is a collapsar, gives a wide range this parameter could take. Siegel et al. (2019) and references therein give one way to calculate a value for this parameter based on the current estimates of GRBs. A long GRB rate of $1.3^{+0.6}_{-0.7} \text{ Gpc}^{-3} \text{ yr}^{-1}$ (Wanderman & Piran 2010), a GRB beaming fraction $f_b \sim 5 \times 10^{-3}$ from an average opening angle $\theta_j = 6^\circ$ (Goldstein et al. 2016), which gives a COL rate of $\sim 260 \text{ Gpc}^{-3} \text{ yr}^{-1}$. With a CCSNe rate of $7.05^{+1.43}_{-1.25} \times 10^4 \text{ Gpc}^{-3} \text{ yr}^{-1}$ (Li et al. 2011), the CCSN per COL is estimated to be ~ 270 . Using this as the f_{COL} value in the above calculations would have lowered the mass of new stars and the time of SF for COLs by a factor of ~ 4 . Earlier work, Paczyński (1998), has a CCSN per COL of $10^4 - 10^5$. These values are just using observed GRB rates, so are underestimates, as not all COLs will be GRBs. A jet-driven supernova could be the result of a COL if the H envelope remained (Heger et al. 2003) so GRB rates are only a bound on the COL rates. MacFadyen & Woosley (1999) has a conservative collapsar estimate of $< 1\%$ of CCSNe, so the parameter would be inverted, > 100 . At a lower metallicity, Heger et al. (2003) predict GRBs and jet-driven SNe are up to $\sim 10\%$ of CCSN, which would make the CCSN per COL as low as 10. The per-galaxy rates of Fryer et al. (1999) have been converted to a CCSN per COL value of between 20–2000. Inverting the f_r of Brauer et al. (2021), they take a fiducial value for this parameter at 10^3 , but investigates a range from 10–10000. These sources give a range of $\log(\text{CCSN per COL})$ from 1 to 5, which is a large spread, explaining why $f_{\text{COL}} = 1000$ was a conservative estimate. In a lower metallicity environment like NGC1569 the lower values for CCSN per COL are acceptable. G22 measures $[\text{Fe}/\text{H}] = -0.74$ for the B cluster presently, and the old stellar population has $-2 < [\text{Fe}/\text{H}] < -1$ (Grocholski et al. 2012). This

low initial metallicity would increase the likelihood of a COL as discussed above, hence a lower CCSN per COL.

2.4.2 CCSN per M_{\odot}

The CCSN per Mass value is dependent on the IMF slope α . This is because a lower α means more high-mass stars are formed, which inherently increases the number of COLs. A standard IMF is that of [Salpeter \(1955\)](#). This has an $\alpha = 2.35$, which gives a CCSN per $M_{\odot} = 7 \times 10^{-3}$ (equation (3)).

The value of α has been shown to vary with SFR. In particular, [Gunawardhana et al. \(2011\)](#) show

$$-\alpha \approx 0.3 \log(\Sigma_{\text{SFR}}) - 1.7 \quad (11)$$

where α is the IMF power law exponent and Σ_{SFR} is the surface density SFR, as above. equation (11) is a sign changed version of equation (14) from [Gunawardhana et al. \(2011\)](#), to agree with the sign convention used here of a positive α . Using the Σ_{SFR} from [Hunter & Elmegreen \(2004\)](#) for NGC1569 of $\Sigma_{\text{SFR}} = 1.29 M_{\odot} \text{ yr}^{-1} \text{ kpc}^{-2}$, equation (11) implies $\alpha = 1.67$. This α gives CCSN per $M_{\odot} = 2.7 \times 10^{-2}$. Changing the IMF is less desirable physically, as [Salpeter \(1955\)](#) was so seminal.

2.4.3 Other parameters

While matching the [Ba/Fe] is important, ignoring all the other outputs of the simulations would invalidate the results. Importantly the metallicity, in [Fe/H]. Before attempting to match the observed [Fe/H], the initial [Fe/H] was the observed value. This did increase with time in the simulations because CCSNe added Fe to the system. Matching the output Fe abundance to the observed value was achieved by changing the initial metallicity value ($[\text{Fe}/\text{H}]_i$) of the merging dwarf galaxies. [Grocholski et al. \(2012\)](#) showed that the old stellar population in NGC1569 has a large metallicity spread in the range of $-2 < [\text{Fe}/\text{H}] < -1$, peaking around -1.25. So initial values from of $[\text{Fe}/\text{H}]_i = -1.2$ and below were tried to find a value that produced a cluster that matched both the observed [Ba/Fe] and [Fe/H]. By lowering this value, the CCSNe can pollute the [Fe/H] to the level observed, -0.74 ± 0.05 from [G22](#), while the COLs do the Ba pollution. This was done in the later models, as trying to match two parameters at once would have been too difficult.

To give some indication of the reliability of the results presented below, the parameters of the dwarf galaxy merger can be changed. The pericentre of the orbit, standard at 8.75 kpc, was varied within about a factor of two. The mass ratio of the two dwarf galaxies, standard at 1:1, was decreased to 1:0.5 for some models. The change in total mass that this causes is not expected to be an issue. Combining changes in both parameters is also explored. The need for a merger is tested by simulating a galaxy in isolation, with otherwise optimal parameters, to see how the SF and r -process pollution is affected.

2.5 Selection of Star Clusters

The new star particles that form can be grouped into clusters after the simulation is complete. Two parameters control the scale of these clusters. The first is a neighbouring radius (NR), which groups stars together if the star particles are all within NR of the centre of mass (COM). The standard value for this is 35 kpc. The other parameter is a threshold identification mass, the group of star particles must have a mass of at least this value within the NR to be a cluster. This is standard at $5 \times 10^5 M_{\odot}$, about the stellar mass of NGC1569-B,

which [Larsen et al. \(2007\)](#) put at $6.1 \times 10^5 M_{\odot}$. NR is only changed if no clusters are detected at the standard value, this is noted in the last column of the results in [Table 1](#). The mass parameter is never changed.

Some groups of stars the simulation identifies as star clusters have intriguing spatial distributions. A distinguishing cut can be made using the potential of the star clusters. The linear regression best-fitting line of radius ($R = \sqrt{x^2 + y^2 + z^2}$) against the measured potential must be negative for a grouping to be a cluster. Any non-negative potential gradient is classed here as an overdensity of stars.

Each star particle in the simulation has a known abundance. Taking the arithmetic mean of star particles in a cluster, the [Ba/Fe] can be compared to that observed in [G22](#) to see if that simulation's set of parameters reproduces a cluster with the super-solar value. This average value is an appropriate way of making the comparison as [G22](#) has measured the [Ba/Fe] from an integrated light spectrum, which has the effect of averaging out the contribution from each star in the cluster. If another way of measuring the Ba abundance was used, i.e. the star with the maximum [Ba/Fe] was taken in each cluster, these results would not be comparable. When a simulation model forms multiple clusters, the one with the highest average [Ba/Fe] is presented as the result. There is no stellar [Ba/Fe] distribution observed in NGC1569-B as individual stars are not resolved in the spectrum. Matching the average value may lead to an understanding, or at least an estimate of, the underlying properties of such a distribution, as the simulations happily provides the data of the abundances for each star particle.

2.6 Parameter Study

[Table 1](#) shows a selection of the simulations performed by this study. In total, we performed 94 simulations, with input values more extreme than shown here, and equally extreme outputs. Those shown in this work have had their model number reindexed to start from M1. The first five simulations shown are representative of those made where the initial [Fe/H] was the value observed in [G22](#). Comparing M2 with M3 and M5, where the CCSN per COL value was held at 100 and the CCSN per M_{\odot} and ρ_{th} were changed, respectively. The [Ba/Fe] changes drastically between these models, so all of these parameters are important. Both M4 and M5 match the observed [Ba/Fe], with completely different parameters. The degeneracy between the two main COL inputs is shown here. This is explained by a lurking variable: COLs per M_{\odot} . It can be derived by dividing the value of CCSN per M_{\odot} by the CCSN per COL value. This lurking variable also explains the same outputs in both M7 & M8 and M13 & M23. Models M6 through M12 show a slow decrease in the initial [Fe/H] values, and the corresponding decrease in the final values.

No matches to both the observed [Ba/Fe] and [Fe/H] values are found until M13. This is the model that has best matched the observed parameters of NGC1569-B. The average [Ba/Fe] and $[\text{Fe}/\text{H}]_f$ match the values observed by [G22](#). This model had the standard high-resolution orbital and merger parameters, threshold gas density $\rho_{th} = 1000 \text{ cm}^{-3}$ and Ba yield from COLs $\text{Ba}/\text{COL} = 2.3 \times 10^{-3} M_{\odot}$. It uses the [Salpeter \(1955\)](#) IMF CCSN per COL of 7×10^{-3} . The initial Fe abundance of $[\text{Fe}/\text{H}]_i = -1.5$ with a CCSN per COL value of 70 was able to match those observations. This initial [Fe/H] is in good agreement with the metallicity of the older star population in NGC1569 [Grocholski et al. \(2012\)](#). This is the model that will be presented for the rest of this work as the fiducial model.

Table 1. A summary highlighting the process done when changing the parameters of the simulation. The key inputs of CCSN per M_{\odot} , CCSN per COL and initial metallicity ($[\text{Fe}/\text{H}]_i$) and shown in columns 2,3 and 5 respectively. The corresponding $[\text{Ba}/\text{Fe}]$ and final metallicity ($[\text{Fe}/\text{H}]_f$) are given in columns 4 and 6. The first column is a model number identifier, and the last column notes if any other parameters have been changed

Model	CCSN per M_{\odot}	CCSN per COL	[Ba/Fe]	$[\text{Fe}/\text{H}]_i$	$[\text{Fe}/\text{H}]_f$	Other Changes
M1	7×10^{-3}	300	0.3 ± 0.1	-0.74	-0.19 ± 0.09	
M2	7×10^{-3}	100	0.6 ± 0.3	-0.74	-0.31 ± 0.06	
M3	7×10^{-3}	100	0.4 ± 0.4	-0.74	-0.3 ± 0.1	low ρ_{th}^a , NR ^b 52.5 pc
M4	7×10^{-3}	30	1.3 ± 0.2	-0.74	-0.22 ± 0.09	
M5	2.7×10^{-2}	100	1.3 ± 0.3	-0.74	-0.27 ± 0.08	
M6	7×10^{-3}	40	1.2 ± 0.4	-1.2	-0.6 ± 0.1	
M7	2.7×10^{-2}	150	1.5 ± 0.3	-1.3	-0.6 ± 0.2	
M8 ^c	7×10^{-3}	40	1.5 ± 0.3	-1.3	-0.6 ± 0.2	
M9	7×10^{-3}	30	– ^d	-1.4	– ^d	ISO ^e
M10	7×10^{-3}	30	1.6 ± 0.2	-1.4	-0.6 ± 0.2	
M11	7×10^{-3}	30	1.4 ± 0.3	-1.5	-0.7 ± 0.1	
M12	7×10^{-3}	50	1.4 ± 0.3	-1.5	-0.6 ± 0.2	
M13	7×10^{-3}	70	1.3 ± 0.2	-1.5	-0.7 ± 0.2	
M14	7×10^{-3}	70	1.3 ± 0.2	-1.5	-0.5 ± 0.2	low ρ_{th}^a , NR 52.5 pc ^b
M15	7×10^{-3}	70	1.3 ± 0.3	-1.5	-0.8 ± 0.2	mass ratio ^f 1:0.5
M16	7×10^{-3}	70	– ^d	-1.5	– ^d	ISO ^e , NR ^b 157.5 pc
M17	7×10^{-3}	70	1.4 ± 0.2	-1.5	-0.7 ± 0.2	pericentre ^g 3.5 kpc
M18	7×10^{-3}	70	1.4 ± 0.3	-1.5	-0.6 ± 0.2	pericentre ^g 17.5 kpc
M19	7×10^{-3}	70	– ^d	-1.5	– ^d	pericentre ^g 3.5 kpc, mass ratio ^f 1:0.5
M20	7×10^{-3}	70	1.3 ± 0.2	-1.5	-0.8 ± 0.1	pericentre ^g 17.5 kpc, mass ratio ^f 1:0.5
M21	7×10^{-3}	70	1.3 ± 0.3	-1.5	-0.7 ± 0.2	pericentre ^g 6.125 kpc
M22	7×10^{-3}	70	1.2 ± 0.5	-1.5	-0.7 ± 0.2	pericentre ^g 13.125 kpc
M23 ^c	2.7×10^{-2}	270	1.3 ± 0.2	-1.5	-0.7 ± 0.2	

^a Low ρ_{th} means the threshold density for star formation in the simulation was decreased from a standard 1000 cm^{-3} to 100 cm^{-3} . ^b NR for neighbouring radius. The distance checked for membership to a cluster, standard at 35 pc. ^c These models output the same data as an earlier model, due to the degeneracy in the parameters CCSN per M_{\odot} and CCSN per COL. The same output for different input parameters highlights the degeneracy well. M8 had the same output as M7, and M23 had the same output as the fiducial model M13. ^d – means the (all the) group(s) of new star particles found had a non-negative potential gradient, and thus failed the check for being a cluster. With no clusters forming, there is nothing to measure the $[\text{Ba}/\text{Fe}]$ of. ^e ISO means there was intentionally no merger in the simulation, the galaxy was isolated. ^f Ratio of the masses of the two galaxies that merge, standard at 1:1. ^g The pericentre distance of the merger orbit, standard at 8.75 kpc.

3 RESULTS

3.1 The Fiducial Model

Fig. 2 describes how numerous young star clusters are formed during the dissipative merging between gas-rich dwarf galaxies in the fiducial model. After the first pericenter passage, the two start to merge to form a single dwarf galaxy with a strong starburst sometime between $T=0.84$ Gyr and 1.12 Gyr. Due to the adopted high gas fractions in the merging of two dwarf galaxies, high-density gaseous regions corresponding to giant molecular clouds can be quickly formed where star formation can proceed very efficiently. Compact stellar systems are consequently formed from the new gas clouds, and some of them can become gravitationally bound star clusters.

Five star clusters are identified in the M13 simulation run, they all lie within the NR of 35 pc, have total stellar masses of more than $5 \times 10^5 M_{\odot}$, and have a negative potential gradient. Two more overdensities are identified, which pass the first two checks, but have a positive potential gradient. The cluster with the highest $[\text{Ba}/\text{Fe}]$ is presented as the best cluster, with a $[\text{Ba}/\text{Fe}] = 1.3 \pm 0.2$ and a $[\text{Fe}/\text{H}]_i = -0.7 \pm 0.2$ matching the observations of G22. The four other star clusters found in the fiducial simulation had similarly high average $[\text{Ba}/\text{Fe}]$ values and distribution, however, the cluster presented as the best cluster had the highest Ba abundance, in accordance with the rest of Table 1. Some other clusters had more new star particles than the best cluster, but similar trends in the other properties.

Fig. 3 shows the abundance distributions of the best cluster for the

key elements in this study. The left panel has the $[\text{Fe}/\text{H}]$ distribution, with the average value in agreement with the measurement in G22 which was a requirement for selecting this as the fiducial model. The spread of the Fe abundance is much larger than the observations, and also larger than typical $[\text{Fe}/\text{H}]$ spreads in GCs. The $[\text{Ba}/\text{Fe}]$ distribution is shown in the centre panel, the average matches the observations, and the spread is of a similar size to what was found in G22. The $[\text{Eu}/\text{Fe}]$, whose average is 1.9 ± 0.2 , provides a good prediction of what this abundance should be in NGC1569-B if the idea of COL pollution is a good model for this cluster's formation. The large spread in Eu is not surprising, like the Fe spread is, as Ba has a large spread in the measurements that are being investigated here and both of these r -process elements are expected to increase in tandem. This $[\text{Eu}/\text{Fe}]$ is higher than anything in the Milky Way for this metallicity (e.g. Suda et al. 2008; Tsujimoto & Shigeyama 2014), but so was the $[\text{Ba}/\text{Fe}]$ abundance that sparked this investigation, so a large Eu abundance was expected. The spread in the Eu abundance is large, but that follows from the large Ba spread. The 60 new star particles are slightly negatively skewed for both the r -process elements, the abundance does not get much higher than the average value, but can get lower.

Only two of these five total clusters can be real, as their density profiles are steep enough, this is shown in Fig. 4. The best SC presented in this work is SC ID 5, and shows a nice fit with the R^{-2} trend lines. The top three clusters in this figure do not have a point in the 0 pc to 2 pc shell, meaning there are no new star particles

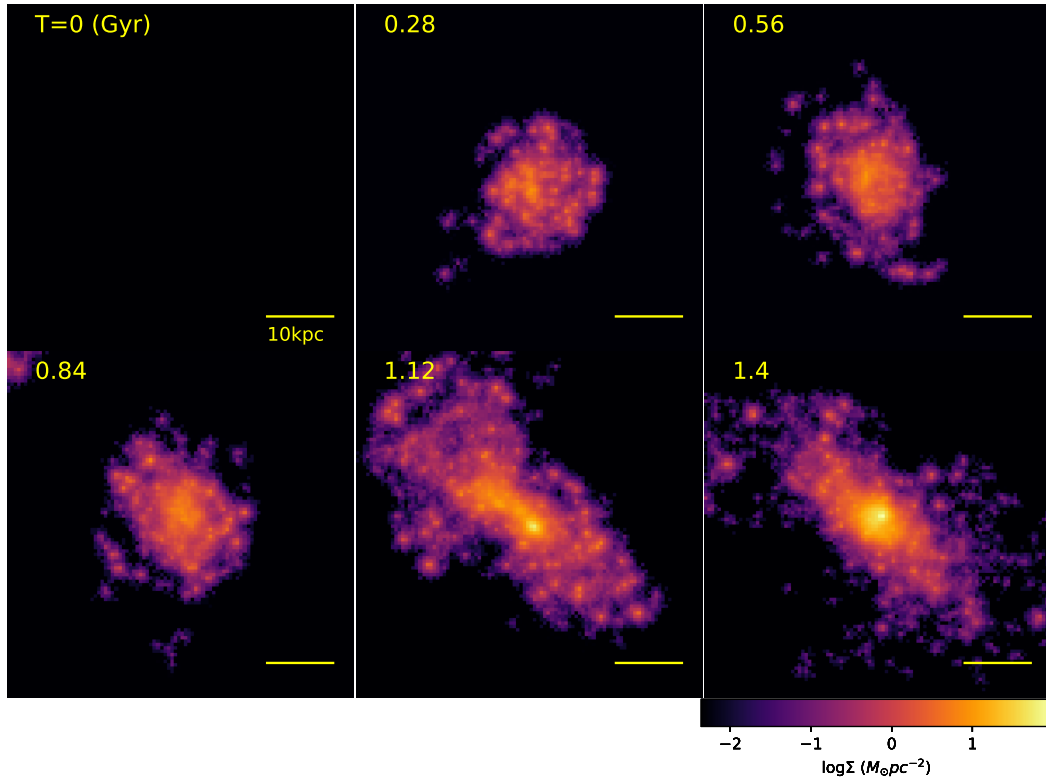


Figure 2. The surface density of new star particles in a log scale, measured in $M_{\odot} \text{pc}^{-2}$, of the fiducial simulation. The six time steps increase by 0.28 Gyr from the start time at $T=0$ in the upper left to $T=1.4$ Gyr lower right. This is centred on one of the dwarf galaxies that are merging. A 10 kpc scale bar is provided in each frame.

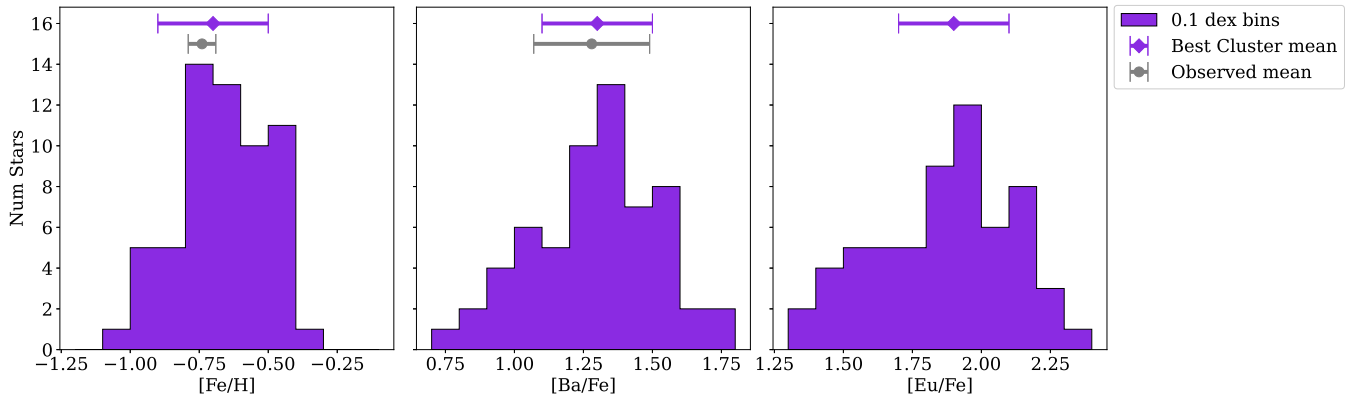


Figure 3. Histogram distributions of (left to right) Fe, Ba and Eu abundances for the best cluster are plotted here. A 0.1 dex bin size is used. The range, not the centring, of each plot is consistent at 1.1 dex for ease of comparison by eye. The purple diamonds with error bars are the mean value of this abundance and its standard deviation. The grey points are the observed values from G22. Note $[\text{Eu}/\text{Fe}]$ was not measured by the observations.

close to the centre of mass (COM) of the system. This means the clusters are not as bound as their negative potential gradient implies. They are unlikely to stay as clusters for long periods of time. The two lower clusters in Fig. 4 have a non-zero density in the first shell, this includes the cluster that has the highest $[\text{Ba}/\text{Fe}]$ of them all. The

SC ID 4 cluster has a larger-than-expected density for most of the shells, however, neither of the lower two SCs have any shells with a density less than the expected trend line. All of these clusters do not follow King profiles (King 1966), their densities have no sharp edges that would be expected of older GCs. These clusters are young, so

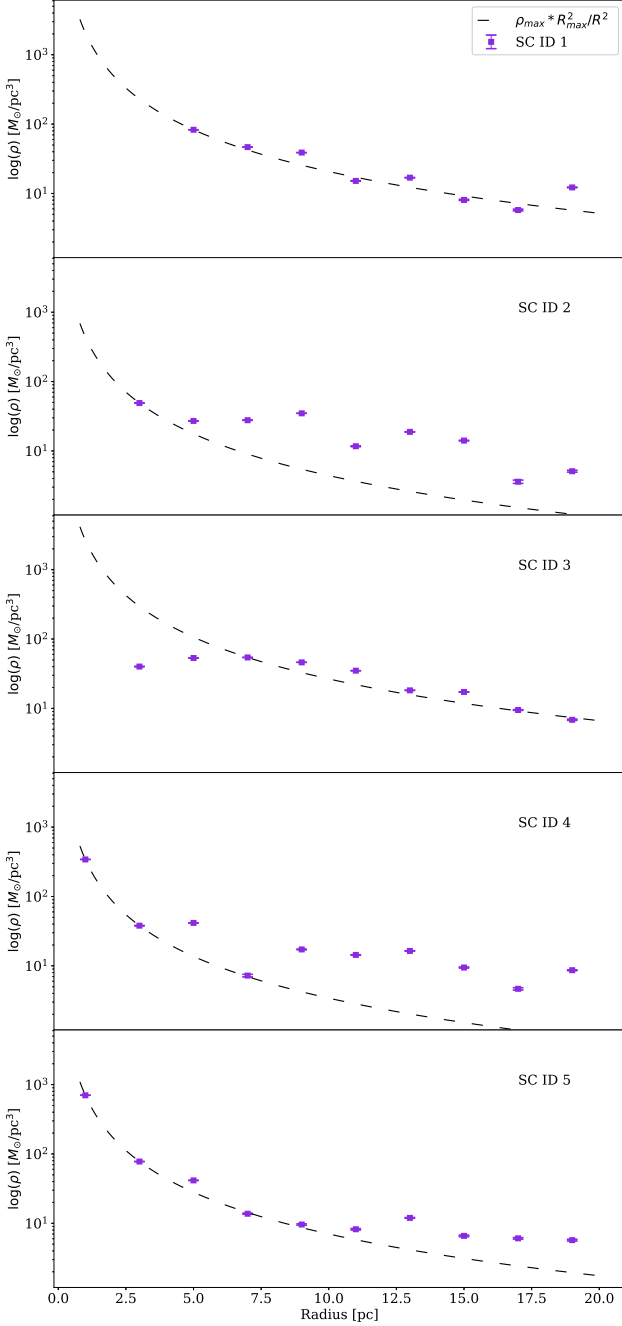


Figure 4. The density of the all the SCs in the fiducial model. The density is plotted on a log scale. Each point (purple squares) are binned in 2 pc spherical shells. The error bars are $\pm \log(1 + \frac{1}{\sqrt{n}})$, where n is the number of star particles in that shell. The dashed black lines are the expected trend, an R^{-2} relationship. These trend lines are scaled to pass through the point of max density, ρ_{max} , at the radius of this maximum, R_{max} .

the tidal force, from the dwarf galaxy they are embedded in these simulations, has not had time to strip the outer star particles.

The abundance gradients of these two clusters are compared in Fig. 5. The best cluster has a mean [Ba/Fe] that is slightly above that of the observations, and the SC ID 4 cluster has a mean that is just lower than both of them, however, they do both agree with the measurement of NGC1569-B's Ba abundance. SC ID 4 has a

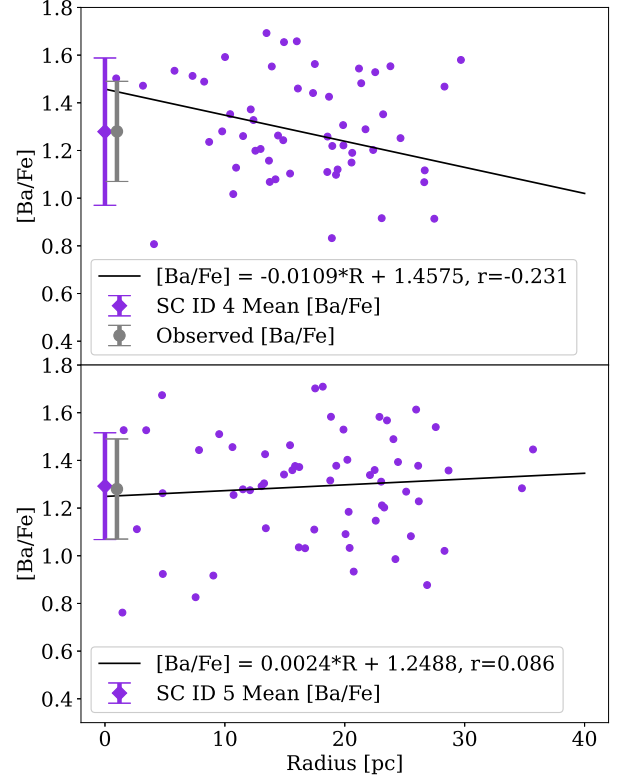


Figure 5. A scatter plot of the [Ba/Fe] abundance against radius from the best cluster's COM. The black line in the best-fitting linear regression to the points, and the legend has the equation of the line and correlation coefficient r . The purple diamond error bar is the cluster's mean [Ba/Fe] and associated standard deviation and the grey circle error bar is the reported [Ba/Fe] of NGC1569-B from G22, as in Fig. 3. The radial positions of these error bars points are just for clarity. The top plot is for the SC ID 4 as in Fig. 4, and the lower plot is for the best SC (ID 5).

rather negative radial Ba gradient, as can be seen from the equation of the best-fitting line, and the correlation coefficient. There is very little correlation between the radius and the Ba abundance in the best cluster, ID 5, as such there is a flat abundance gradient. This highlights that it is the entire cluster has a high [Ba/Fe], and the average is not being raised by a few outliers.

When considering all the newly formed star particles instead of just the best cluster, similar distributions to those in Fig. 3 can be made. For the fiducial model, this is shown in the top (hatched green) of Fig. 6. The iron abundance is heavily unimodal, and the number of stars at higher metallicity decreases quickly. The mode at the minimum value is more than twice the height of the other bars. This is contrasted by both r -process elements, which both show one mode at the minimum value and then peak again at around the values of the chosen cluster. The other clusters found in this simulation, which also had rather high [Ba/Fe], are accounted for in the positive mode of these plots. This bimodality is interesting and reinforces that the best cluster is not an anomaly, and this model of COL pollution of the r -process is viable. They produce a lot of these heavier elements quickly, and when so many of them occur because of a burst of SF at low metallicity there can be clusters with a high r -process abundances when a second round of star formation happens. The spread is reflected in the uncertainty in the mean of each element.

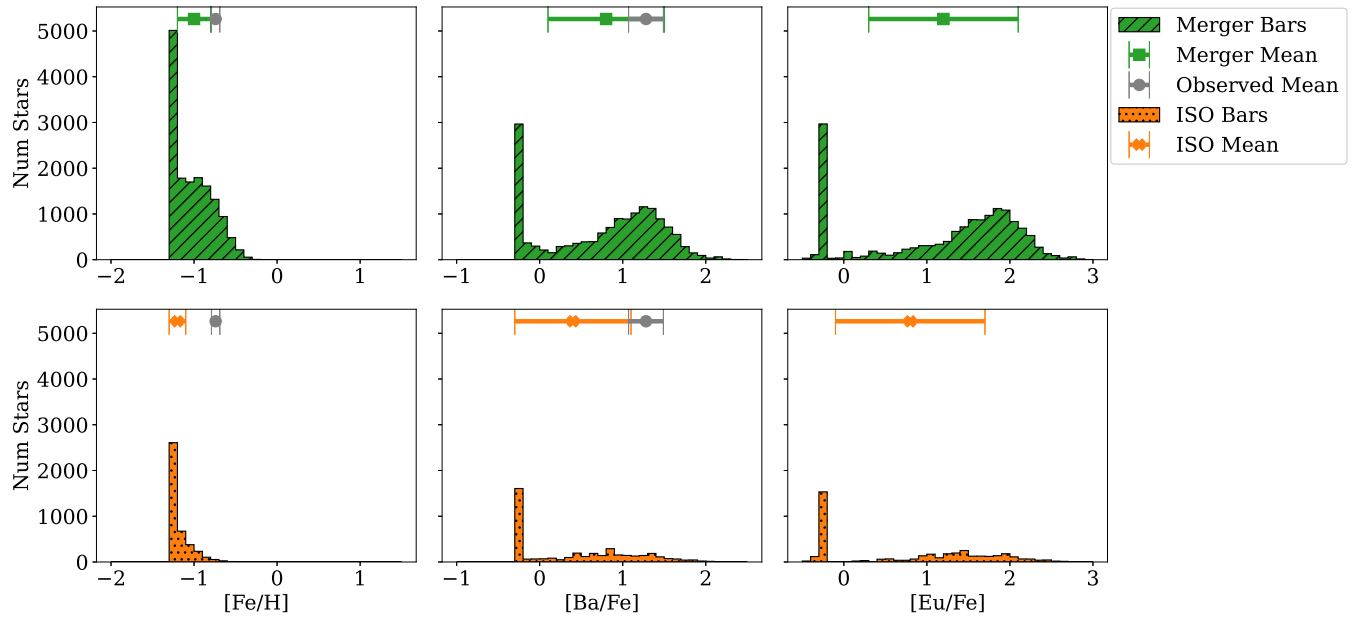


Figure 6. Similar to Fig. 3 but for all the new star particles in the fiducial merger simulation M13 (hatched green, top row), not just the best cluster, and all the new star particles in the isolated galaxy simulation M16 (dotted orange, bottom row). The averages for the merger model is shown with the green squares, and for the isolated model in the orange crosses. The bin size is still 0.1 dex. However, the bars appear thinner as the range of values is now 3.5 dex to show the range of [Eu/Fe].

The [Ba/Fe] has a large spread, which encompasses the observational value, but this observed value is well-constrained enough that there is no overlap from the observational error bars, so the values do not agree.

The lowest abundances of each plot in the top row of Fig. 6 are slightly above the value set as the minimum, most clearly in the [Fe/H] plot. The $[\text{Fe}/\text{H}]_i$ was set to -1.5 to match the observations in the cluster that formed. The mode of the iron distribution is in the bin centred on -1.25. There are bins with a lower metallicity than this available, but they are not populated by any new stars. This can be explained by the evolution of the star particles that existed at the start of the simulation. As star formation was gradual at first, as shown in Fig. 2, the old star particles had time to evolve and increase the metallicity of the system before any new stars were formed. Most of the new star particles in the peak at the minimum would have been formed in the first burst of SF, and the ones that form the clusters are in the higher peaks of the r -process elements.

3.2 Parameter Dependence

Having found a fiducial model (M13 of Table 1) that matched the observations of G22, our attention turned to understanding the effects of the assumptions of the other parameters of the simulations. These tests show that the parameters that had been assumed have at most a small effect on the results, shown in Table 1 for models M14–M22. These models have the same CCSN per M_{\odot} , and CCSN per COL as the fiducial model, the changes made to each model are detailed in the ‘‘Other Changes’’ column of Table 1. We now describe each of the changes, and their effects, in turn.

The largest effect is decreasing the threshold gas density, ρ_{th} , to 100 cm^{-3} . As shown by M14 in Table 1, this changes the [Fe/H] significantly, $[\text{Fe}/\text{H}]_f = -0.5 \pm 0.2$, placing on the upper edge of the uncertainty limit from the fiducial model. This cluster did require a

slightly larger NR to be detected, 52.5 pc which is 1.5 times larger than the standard 35 pc. M14 has more than twice as many new star particles form than the fiducial simulation, yet they aren’t clustered. Only one cluster was formed at this larger NR, it passes the potential gradient check but does not have any star particles within 10 pc of the COM, making the shell density against radius rather empty. It seems the lower ρ_{th} makes it easier for stars to form, as expected, but harder for clusters to form. This may be due to the density of nearby gas particles influencing each other. It is more likely that a group of particles will all approach the higher density together, encouraging cluster formation. While perhaps an individual particle can reach the lower value on its own and the feedback from the new young stars could lower the density of the surrounding gas, which decreases clustering tendencies.

The initial mass ratio of the two galaxies was also investigated. For M15, the ratio was changed to 1:0.5. This does lower the total mass in the system, by a factor of $\frac{1}{4}$ for the ratio used. However, it seems to not affect the [Ba/Fe] value, indicating that the SF is brought on by the merger and the total mass of the system is less important. Three clusters pass the negative potential gradient check, but none have a non-zero density near the COM.

The ‘ISO’ tag in M9 and M16 means there was no merger initialised, just leaving the one dwarf galaxy to evolve on its own. These models failed to produce a cluster, even at an extreme NR of 157.5 pc, more than 4 times the standard value. With nothing to promote SF, it makes sense that there would not be a new cluster of stars in this small galaxy. The bottom row (dotted orange) of Fig. 6 shows the abundance distribution of the new stars in the isolated model with otherwise fiducial parameters, M16. There are 3 times fewer new star particles than in the merger model (shown above), the majority of these stars are at the minimum abundance for each element. This demonstrates that a merger drives the starburst and leads to cluster formation as no cluster was found in M16 even with a large NR.

The pericentre distance is standard at 8.75 kpc, models that vary just this parameter (M17, M18, M21 and M22), show good agreement with the fiducial model. This means the result of the fiducial simulation is rather invariant under a change of pericentre of the merger. The changes in both the barium and iron abundances are only 0.1 dex, which is within the uncertainties of these measurements. There seems to be no trend in the number of SCs that pass the negative potential gradient check and the pericentre distance. Only in M21 is there no SC that has a well-fitting $\rho \propto R^{-2}$ cluster, the rest of the models had at least one.

The pericentre changes can be combined with a mass ratio change. The ‘-’ of M19, from no grouping of new star particles passing the negative potential gradient check, is interesting because it combines two changes that both successfully formed clusters. The larger pericentre of M20 with the lower mass ratio had outputs in agreement with the fiducial model, so there should not be too large of an effect for any changes in these parameters on the abundances. However, this model only had one cluster pass the potential gradient check, and it has no star particles within the first 2 pc. It seems that the stars will form with high Ba abundances, but the merger parameters seem to disfavour mergers.

The only 0.1 dex variance in the abundance outputs as sensitivity to any of the merger parameters from these models is a positive result. The lack of clustering in some of these models is of slight concern. However, this work did not attempt to find any exact orbital merger history of NGC1569. Instead, the merger was used to excite the high SFR, needed for COL pollution, as seen in the bursty SFH of NGC1569 (Angeretti et al. 2005). The invariance shown in the abundances solidifies that it is the COL rates that are important, not the specific merger parameters. The mergers simulated here have old star particles in both bodies, but there is no *a priori* reason that this is required. This merger need not be with a galaxy, it could just be an HI cloud, which fits slightly better with the results of Johnson (2013).

The M23 was designed to show the degeneracy between the CCSN per M_{\odot} and CCSN per COL values. The COL per M_{\odot} value, the lurking variable in these simulations as it is not an explicit input, are the same, 1×10^{-4} . Interestingly, the value of this lurking variable is such a round number. The flag of this model in Table 1 indicates congruence with M13. I.e. the same number of new star particles and clusters were formed in both. It is not just that the [Ba/Fe] is the same, they were the exact same simulation, despite the difference in input parameters. This was the expected behaviour because this run was designed to have the same value of COL per M_{\odot} for a different IMF, one that is physically motivated, and derived from equation (11). The fiducial model does have the benefit that it has a standard (Salpeter 1955) IMF. It shows that the fiducial simulation is not the only set of parameters that works. Any combination of CCSN per M_{\odot} and CCSN per COL that have a ratio of 1×10^{-4} would give the same result. It is interesting to note that this model has a CCSN per COL that matches the current GRB rate estimates, as described in subsection 2.4.

4 DISCUSSION

4.1 Unresolved problems in COL scenario

Although we have provided a reasonable explanation for the observed high [Ba/Fe] of NGC1569 B and theoretical predictions (e.g., [Eu/Fe]) of other properties of the SC, we here list several unresolved problems of the proposed COL scenario.

4.1.1 Very high [Cr/Fe] and [Sc/Fe]

There are other anomalous abundances of NGC1569-B as reported in G22. The [Cr/Fe] = 0.50 ± 0.11 and the [Sc/Fe] = 0.78 ± 0.20 are both higher than expected, but not nearly as extreme as the [Ba/Fe] measurement that our study has focused on. The high [Cr/Fe] could be explained if the yield of Cr in COLs are close to that of MR-SNe yields for this element. G22 does state that the Sc value is particularly uncertain. The spread is discussed at length with the changes to the measurement when fitting fewer Sc lines shown, but if the measurement is to be believed then the abundance contributions from massive stars, type Ia, and type II supernova would have to be different from the Milky Way and other galaxies. The spread in [Ba/Fe] is not mentioned in the text merely shown in a table in the appendix. COLs have a difficult job explaining this Sc overabundance analytically.

Iliadis et al. (2016) show that super-AGB stars or novae of CO or ONe white dwarfs are sites that can produce high Sc pollution. However, the timescale of the white dwarf novae is slightly too long for NGC1569-B; at least 100 Myr. This is longer than the current age of the cluster, and having earlier SF do this pollution would be challenging because of the spatial extents of these bursts. We suggest that these super-AGB stars can pollute the ISM before cluster formation. Much like the COLs, these stars would have been formed in the earlier round of starburst, super-AGB stars are active on timescales 30 Myr, slightly longer than COLs which casts doubt on whether they would be a good candidate. Super-AGB stars would also force the K abundance to be high, as the Mg-K anticorrelation presented in Iliadis et al. (2016) would take the [Mg/Fe] 0.22 ± 0.05 of G22 to a [K/Fe] of about 1.5. G22 did not measure the [K/Fe] of NGC1569-B, so there is currently no way of knowing this abundance. A mixture of COL and super-AGB ejecta could be an interesting explanation of the mix of high values of Sc, Cr and Ba abundances.

4.1.2 Fe spread

The final [Fe/H] value for the fiducial model is -0.7 ± 0.2 , and this uncertainty of 0.2 dex is a large dispersion for a Fe abundance among the new star particles in the cluster. The left panel of Fig. 3 shows this larger scatter in the [Fe/H] values in histogram form. G22 measured [Fe/H] = -0.74 ± 0.05 , with the ± 0.05 being a measurement uncertainty, not a dispersion, as the integrated light spectra technique used does not measure the [Fe/H] (or any abundance) for individual stars. The COL model seems to produce this large spread in Fe naturally. The AGB pollution discussed above would give a small Fe spread, as these stars have no Fe in their ejecta. If the timescales worked in their favour, (super-)AGB stars could be preferred over COLs, but NGC1569-B is too young. The high spread in [Fe/H] is a prediction of the model. While observations of this dispersion would be challenging due to technological limitations, any measurements made would be useful to check the validity of the model.

4.1.3 Parameter degeneracy

The number of COLs that occur is the important value, but it is highly degenerate. Two ways of increasing this number have been explored, changing the CCSN per COL input and changing the IMF, achieved by changing the CCSN per M_{\odot} input. The former increases this total number of COLs because COLs are more common, observationally this is linked to the number of long GRBs. The latter is increasing the number of CCSNe, which can result in the same number of COLs with a lower fraction of CCSN being COLs. This is dependent on the

IMF power law exponent changing with SFR, which there is some evidence for (Gunawardhana et al. 2011).

The degeneracy between these parameters is very strong, as discussed above the lurking variable of COL per M_{\odot} explains the degeneracy. There is hope to break it, but not through these simulations, only with further study into both SFR-dependent IMFs and GRB frequencies. If it is found that a low CCSN per COL is acceptable, meaning there are more long GRBs observed, then a Salpeter (1955) IMF works well with these results, as the observations can be reproduced with a CCSN per COL of 70, the value of this parameter in the fiducial model, about $\frac{1}{4}$ the estimated rate (see subsection 2.4). The higher GRB rate may only need to be acceptable at lower metallicities. The current estimates are for the local universe, which is not metallicity specific. If there are the current estimates on the GRB frequencies are overestimates, i.e. they predict more GRBs than are observed even at low metallicities, an SFR-dependent IMF is needed to reproduce the observed [Ba/Fe], as seen in M23.

4.1.4 Origin of High COL fraction

It remains unclear why rotating massive stars can be formed efficiently in a dwarf galaxy merger environment. The CCSN per COL value of the fiducial model (70) is towards the lower end of the physically applicable range. This is about a factor of 4 lower than the current GRB estimates would have, which is ~ 270 (see subsection 2.4). One has to wonder how these COLs would have formed so efficiently. Lowering the initial metallicity of the system does improve the chances of massive stars being COLs due to previously discussed reasons to do with the predicted rotation rates of WR stars (see subsection 2.1.1). At such an initial [Fe/H] to reproduce the observed [Fe/H] of NGC1569, the CCSN per COL values used in the fiducial simulation of 70 are well within the range predicted by Heger et al. (2003) of $\sim 10\%$ of CCSN being COLs. The high SFR of the simulations at a low metallicity also helps the model as all the COLs can form in optimal conditions, and the star clusters form afterwards. The SFH of NGC1569-B as described by Angeretti et al. (2005), with three intense bursts in recent history, is consistent with these results. The first burst would have formed the COLs, and the latest would have formed the cluster.

4.2 Is NGC1569-B unique?

Milky Way GCs (e.g. Larsen et al. 2017) and those in dwarf galaxies (e.g. Larsen et al. 2012, 2014; Gvozdenko et al. 2024) have [Ba/Fe] much lower than observed in G22, when all were observed with the same technique of an integrated light spectrum. This suggests that the COL pollution proposed here is unique to NGC1569-B. The GCs in our galaxy could have been formed in isolation during dwarf galaxy formation before being captured into the Milky Way, and this difference in the SF environment could go some way to explaining the difference. The high CCSN per COL fraction needed for the fiducial model presented in this work is questionable to have only occurred once, but the same problem exists for any explanation of such a seemingly unique abundance. Our presented CCSN per COL value, 70, being only a factor of about 4 lower than the GRB estimated rate puts it well within the bounds of possibility. Observations of long GRB host galaxies could be crucial, if the hosts preferentially show evidence of mergers then the COL fraction could be higher after a merger.

The bursty SFH of NGC1569 may be such that there was the correct number of COLs formed in the lifetime of the GMC. This can be seen

in greater significance by using the parameter of the fiducial model, $f_{\text{COL}} = 70$, in equation (2), equation (5) and equation (6). The values become $M_{*, \text{COL}} = 1.8^{+1.2}_{-0.7} \times 10^6 M_{\odot}$ and $\Delta t_{\text{SF, COL}} = 3.8^{+2.5}_{-1.6}$ Myr. These are even more in favour of the COL model than our original estimates, with the SF time being well less than the lifetime of a GMC. This is without even considering the complicating effects of lowering the initial metallicity, which lowers the required number of COLs and makes them more likely. Therefore, SF before the -B cluster formed is certainly enough to pollute the GMC. The unique circumstances of the merger into a bursty SFH and then forming an SSC that is bright enough to observe from Earth are all compounding factors into this [Ba/Fe] being so high. The other GCs mentioned above may have formed with less erratic histories and thus a lower Ba abundance as there would have not been enough SF right before their GMCs collapsed to have enough COLs occur for the r -process pollution.

4.3 Future work

There was no attempt to make mock observations of the clusters detected in the simulations, these would be a good progression to this work to see if the results are still valid. By taking an integrated light spectrum of the clusters identified in the simulations, a more self-consistent comparison of the abundances can be made. Any systematic errors would be present in both the real and the mock spectra, and the biases of taking the mean of all the star particles could be removed. While averaging the abundance of each star particle in principle has a similar effect to a spectrum of all the light, no weighting of the intrinsic brightness of each star is taken into account. The colour-magnitude diagram (CMD) binning that the integrated light spectra analysis performs does take stellar spectral type into account (Larsen et al. 2012). This would be the difficult step of taking these mock measurements, as the star particles in the simulation represent more than one star. The CMD binning makes less sense at this resolution, and finding a way around this problem is left for future work as it is outside the scope of this work.

Taking the average is not the worst choice we could have made, instead the highest single star particle's [Ba/Fe] could have been chosen for each cluster. As shown in Fig. 3 that would lead to ~ 0.5 dex higher abundances, which would have skewed the input parameters to prefer fewer COLs. While we are confident in our results from the averages alone, the mock observation technique would be a good extension.

Another opportunity for more research would be taking follow-up observations of NGC1569-B and -A. This work predicts the [Eu/Fe] value of the -B cluster ([Eu/Fe] = 1.9 ± 0.2) and an attempt to verify this prediction is needed to determine if these simulations accurately describe the cluster. The COL pollution model as a concept would predict the -A cluster would also have a large r -process abundances, as the initial conditions of the ISM and the merger and SFH are the same. The simulations back this theory up, with most models having a few more clusters with [Ba/Fe] within 0.2 dex of the presented cluster. Performing these observations is not in our expertise, but any attempts to do so are welcome.

5 CONCLUSION

The massive star cluster NGC 1569-B is observed to have unique chemical abundance patterns in its stars, in particular, extremely high [Ba/Fe] of 1.28 ± 0.21 (G22). We consider that this Ba is of r -process origin due to chemical enrichment by COLs, NSMs or

MR-SNe. Accordingly, we have investigated the required number of each of these r -process sites and some properties of the SF needed to produce them. We then investigated the star cluster formation from merging dwarf galaxies in the context of the COL scenario using supercomputer simulations of the chemodynamical evolution, with COLs being the r -process synthesizers.

(i) The number of events needed to pollute a GMC up to the correct [Ba/Fe] levels vary between the different r -process sites. Collapsars requires $M_{*,\text{COL}} = 2.6_{-1.1}^{+1.7} \times 10^7 M_{\odot}$ of stars need to form, and this takes $\Delta t_{\text{SF,COL}} = 53_{-22}^{+36}$ Myr at the current SFR ($0.48 M_{\odot} \text{ yr}^{-1}$ Hunter & Elmegreen 2004). This time is consistent with the SFH of NGC1569 (Angeretti et al. 2005), which implies COLs are a good candidate for the r -process pollution of NGC1569-B.

(ii) The number of MR-SNe needed is high, and so the corresponding mass of stars that need to form and the time of SF is inconsistent with the SFH of the galaxy. The old stellar population in NGC1569 is expected to have 84 NSMs occur during the lifetime of the GMC that formed the -B cluster, when the number required for the Ba pollution is orders of magnitudes greater. Therefore, we reject these other sites for the r -process pollution of NGC1569-B and conclude that COLs must do this pollution.

(iii) Star clusters can be formed in dwarf galaxy mergers, and we had a cluster match the observed properties of NGC1569-B. The main result was that a [Ba/Fe] = 1.3 ± 0.2 and a [Fe/H] = -0.7 ± 0.2 , matching the G22 observation. This was achieved with a standard Salpeter (1955) IMF, an initial metallicity of [Fe/H]_i = -1.5 and a CCSN per COL of 70, which is only a factor of 4 lower than current long GRB rates would put it. The best cluster has a negative potential gradient, as was required, and a slight negative skew in the r -process element distributions. We have shown these findings are robust to changes in the parameters of the dwarf galaxy merger, but that a merger of some kind is necessary.

(iv) NGC1569-B did not have an Eu abundance measurement made. However, our simulations did measure the [Eu/Fe] of the clusters. From the fiducial model, a prediction of the Eu abundance of the real SSC is made; [Eu/Fe] = 1.9 ± 0.2 . Follow-up measurements of Eu are needed to confirm or refute this result.

(v) The degeneracy between the simulation input parameters of CCSN per M_{\odot} and CCSN per COL was the main issue with this study. Another cluster fits the observations with an SFR derived IMF and an observational CCSN per COL value. The lurking variable of COLs per M_{\odot} is what controlled our results, even though it was not an explicit input, but there is hope to break the degeneracy with more work.

(vi) While we are confident in our results, there is still work to be done. A mock observation of the simulations to get a better comparison to real world data through integrated light spectra would be a great step to take. To achieve this a consideration of the CMD of a simulated cluster is required.

ACKNOWLEDGEMENTS

BL would like to thank ICRAR for the opportunity to be a part of their summer studentship program.

This work was performed on the OzSTAR national facility at Swinburne University of Technology. The OzSTAR program receives funding in part from the Astronomy National Collaborative Research Infrastructure Strategy (NCRIS) allocation provided by the Australian Government, and from the Victorian Higher Education State Investment Fund (VHESIF) provided by the Victorian Government.

DATA AVAILABILITY

The data used for this work will be made available on reasonable request.

REFERENCES

- Abbott B., et al., 2017, *Physical Review Letters*, 119, 161101
 Aloisi A., et al., 2001, *The Astronomical Journal*, 121, 1425
 Anand S., et al., 2024, *The Astrophysical Journal*, 962, 68
 Anders P., de Grijs R., v. Alvensleben U. F., Bissantz N., 2004, *Monthly Notices of the Royal Astronomical Society*, 347, 17
 Angeretti L., Tosi M., Greggio L., Sabbi E., Aloisi A., Leitherer C., 2005, *The Astronomical Journal*, 129, 2203
 Arnould M., Goriely S., Takahashi K., 2007, *Physics Reports*, 450, 97
 Barnes J. E., 2004, *Monthly Notices of the Royal Astronomical Society*, 350, 798
 Barnes J., Duffell P. C., 2023, *The Astrophysical Journal*, 952, 96
 Barnes J., Metzger B. D., 2022, *The Astrophysical Journal Letters*, 939, L29
 Bastian N., Lardo C., 2018, *Annual Review of Astronomy and Astrophysics*, 56, 83
 Bekki K., 2008, *MNRAS*, 388, L10
 Bekki K., 2013, *Monthly Notices of the Royal Astronomical Society*, 432, 2298
 Bekki K., 2014, *Monthly Notices of the Royal Astronomical Society*, 438, 444
 Bekki K., 2015, *Astrophysical Journal Letters*, 812, L14
 Bekki K., Mackey A. D., 2008, *MNRAS*, 394, 124
 Bekki K., Tsujimoto T., 2017, *The Astrophysical Journal*, 844, 34
 Bekki K., Forbes D. A., Beasley M. A., Couch W. J., 2002, *Monthly Notices of the Royal Astronomical Society*, 335, 1176
 Bekki K., Beasley M. A., Forbes D. A., Couch W. J., 2004, *The Astrophysical Journal*, 602, 730
 Bell R. A., Dickens R. J., 1980, *The Astrophysical Journal*, 242, 657
 Blanchard P. K., et al., 2024, *Nature Astronomy* 2024 8:6, 8, 774
 Brauer K., Ji A. P., Drout M. R., Frebel A., 2021, *The Astrophysical Journal*, 915, 81
 Carretta E., Bragaglia A., 2021, *Astronomy & Astrophysics*, 646, A9
 Carretta E., et al., 2009, *A&A*, 505, 117
 Carretta E., Bragaglia A., Gratton R. G., Recio-Blanco A., Lucatello S., D’Orazi V., Cassisi S., 2010, *Astronomy and Astrophysics*, 516, A55
 Cortijo-Ferrero C., et al., 2017, *Astronomy & Astrophysics*, 607, A70
 Cowan J. J., Sneden C., Lawler J. E., Aprahamian A., Wiescher M., Langanke K., Martínez-Pinedo G., Thielemann F.-K., 2021, *Reviews of Modern Physics*, 93, 015002
 Crowther P. A., 2007, *Annual Review of Astronomy and Astrophysics*, 45, 177
 Fryer C. L., Woosley S. E., Hartmann D. H., 1999, *The Astrophysical Journal*, 526, 152
 Goldstein A., Connaughton V., Briggs M. S., Burns E., 2016, *The Astrophysical Journal*, 818, 18
 Gratton R., Sneden C., Carretta E., Gratton R., Sneden C., Carretta E., 2004, *ARA&A*, 42, 385

- Gratton R. G., Carretta E., Bragaglia A., 2012, *Astronomy and Astrophysics Review*, 20, 1
- Gratton R. G., et al., 2015, *Astronomy and Astrophysics*, 573, A92
- Grocholski A. J., et al., 2008, *The Astrophysical Journal*, 686, L79
- Grocholski A. J., van der Marel R. P., Aloisi A., Annibali F., Greggio L., Tosi M., 2012, *The Astronomical Journal*, 143, 117
- Gunawardhana M. L. P., et al., 2011, *Monthly Notices of the Royal Astronomical Society*, 415, 1647
- Gvozdenko A., Larsen S. S., Beasley M. A., Brodie J., 2022, *Astronomy & Astrophysics*, 666, A159
- Gvozdenko A., Larsen S. S., Beasley M. A., Cabrera-Ziri I., Eitner P., Battaglia G., Leaman R., 2024, *Astronomy and Astrophysics*, 685, A154
- Heger A., Fryer C. L., Woosley S. E., Langer N., Hartmann D. H., 2003, *The Astrophysical Journal*, 591, 288
- Hunter D. A., Elmegreen B. G., 2004, *The Astronomical Journal*, 128, 2170
- Iliadis C., Karakas A., Prantzos N., Lattanzio J., Doherty C., 2016, *ApJ*, 818, 98
- Israel F. P., 1988, *Astronomy and Astrophysics* (ISSN 0004-6361), vol. 194, no. 1-2, April 1988, p. 24-32., 194, 24
- Johnson M., 2013, *The Astronomical Journal*, 145, 146
- Johnson M., Hunter D. A., Oh S.-H., Zhang H.-X., Elmegreen B., Brinks E., Tollerud E., Herrmann K., 2012, *The Astronomical Journal*, 144, 152
- Kennicutt R. C. J., 1998, *The Astrophysical Journal*, 498, 541
- King I. R., 1966, *AJ*, 71, 64
- Kirby E. N., Duggan G., Ramirez-Ruiz E., Macias P., 2020, *The Astrophysical Journal Letters*, 891, L13
- Kirby E. N., Ji A. P., Kovalev M., 2023, *The Astrophysical Journal*, 958, 45
- Kohri K., Narayan R., Piran T., 2005, *The Astrophysical Journal*, 629, 341
- Lahén N., Naab T., Szécsi D., 2024, *MNRAS*, 530, 645
- Larsen S. S., Origlia L., Brodie J., Gallagher J. S., 2007, *Monthly Notices of the Royal Astronomical Society*, 383, 263
- Larsen S. S., Brodie J. P., Strader J., 2012, *Astronomy & Astrophysics*, 546, A53
- Larsen S. S., Brodie J. P., Forbes D. A., Strader J., 2014, *Astronomy & Astrophysics*, 565, A98
- Larsen S. S., Brodie J. P., Strader J., 2017, *Astronomy & Astrophysics*, 601, A96
- Li W., Chornock R., Leaman J., Filippenko A. V., Poznanski D., Wang X., Ganeshalingam M., Mannucci F., 2011, *Monthly Notices of the Royal Astronomical Society*, 412, 1473
- MacFadyen A. I., Woosley S. E., 1999, *The Astrophysical Journal*, 524, 262
- MacFadyen A. I., Woosley S. E., Heger A., 2001, *The Astrophysical Journal*, 550, 410
- Marino A. F., Milone A. P., Piotto G., Villanova S., Bedin L. R., Bellini A., Renzini A., 2009, *A&A*, 505, 1099
- McKenzie M., Bekki K., 2018, *Monthly Notices of the Royal Astronomical Society*, 479, 3126
- McLaughlin G., Surman R., 2005, *Nuclear Physics A*, 758, 189
- McQuinn K. B. W., et al., 2010, *The Astrophysical Journal*, 721, 297
- Meléndez J., Cohen J. G., 2009, *The Astrophysical Journal*, 699, 2017
- Miller J. M., Sprouse T. M., Fryer C. L., Ryan B. R., Dolence J. C., Mumpower M. R., Surman R., 2020, *The Astrophysical Journal*, 902, 66
- Mouschovias T. C., Tassis K., Kunz M. W., 2006, *The Astrophysical Journal*, 646, 1043
- Mucciarelli A., Bellazzini M., Ibata R., Merle T., Chapman S. C., Dalessandro E., Sollima A., 2012, *Monthly Notices of the Royal Astronomical Society*, 426, 2889
- Mösta P., Roberts L. F., Halevi G., Ott C. D., Lippuner J., Haas R., Schnetter E., 2018, *The Astrophysical Journal*, 864, 171
- Navarro J. F., Frenk C. S., White S. D. M., 1996, *The Astrophysical Journal*, 462, 563
- Nishimura N., Sawai H., Takiwaki T., Yamada S., Thielemann F.-K., 2017, *The Astrophysical Journal Letters*, 836, L21
- O'Connell R. W., John S. I. G., Hunter D. A., 1994, *The Astrophysical Journal*, 433, 65
- Osborn W., 1971, *The Observatory*, 91, 223
- Paczynski B., 1998, *The Astrophysical Journal*, 494, L45
- Pancino E., et al., 2017, *Astronomy and Astrophysics*, 601, A112
- Pearson W. J., et al., 2019, *Astronomy & Astrophysics*, 631, A51
- Pruet J., Thompson T. A., Hoffman R. D., 2004, *The Astrophysical Journal*, 606, 1006
- Roederer I. U., 2011, *The Astrophysical Journal*, 732, L17
- Salpeter E. E., 1955, *The Astrophysical Journal*, 121, 161
- Sana H., et al., 2012, *Science*, 337, 444
- Schweizer F., 2005, in De Grijs R., González Delgado R. M., eds, *Starbursts*. Springer Netherlands, Dordrecht, pp 143–152, doi:10.1007/1-4020-3539-X_25
- Siegel D. M., 2022, *NatRP*, 4, 306
- Siegel D. M., Barnes J., Metzger B. D., 2019, *Nature*, 569, 241
- Snedden C., Kraft R. P., Prosser C. F., Langer G. E., 1992, *AJ*, 104, 2121
- Stil J. M., Israel F. P., 1998, *Astronomy and Astrophysics*, 337, 64
- Suda T., et al., 2008, *Publications of the Astronomical Society of Japan*, 60, 1159
- Tarumi Y., Yoshida N., Inoue S., 2021, *The Astrophysical Journal Letters*, 921, L11
- Tsujimoto T., Shigeyama T., 2014, *Astronomy & Astrophysics*, 565, L5
- Tsujimoto T., Nishimura N., Tsujimoto T., Nishimura N., 2015, *ApJL*, 811, L10
- Tsujimoto T., Matsuno T., Aoki W., Ishigaki M. N., Shigeyama T., 2017, *The Astrophysical Journal Letters*, 850, L12
- Wanderman D., Piran T., 2010, *Monthly Notices of the Royal Astronomical Society*, pp no–no
- Williams M. L., Bekki K., McKenzie M., 2022, *Monthly Notices of the Royal Astronomical Society*, 512, 4086
- Woosley S. E., 1993, *The Astrophysical Journal*, 405, 273
- Woosley S. E., Bloom J. S., 2006, *Annual Review of Astronomy and Astrophysics*, 44, 507
- Worley C. C., Hill V., Sobek J., Carretta E., 2013, *Astronomy & Astrophysics*, 553, A47
- Zenati Y., Siegel D. M., Metzger B. D., Perets H. B., 2020, *Monthly Notices of the Royal Astronomical Society*, 499, 4097

This paper has been typeset from a $\text{\TeX}/\text{\LaTeX}$ file prepared by the author.